Development of Near-Surface Alloy Composition Anomaly

Yong W. Kim
Department of Physics, Lehigh University
Bethlehem, Pennsylvania 18015 USA

Abstract

Many multi-element alloy specimens have been shown to possess a wide variety of near-surface elemental composition profiles, which are significantly different from the bulk composition. Such composition non-uniformity adversely affects the measurement of basic thermophysical properties in alloys. In this paper we present a new investigation into the mechanisms by which such depth-dependent near-surface elemental composition develops. Specifically, specimens of a low melting-point metallic alloy, Wood's alloy, as a model system are examined under varying thermal cycling conditions within a chamber of controlled gaseous atmosphere. The near-surface composition and thermal diffusivity are measured as a function of depth. The method of time resolved spectroscopy of laser-produced plasma plumes emanating from the specimen surface is used. We show that different surface composition profiles emerge depending on the dynamic range of the thermal cycling forced on a specimen.

1. Introduction

Strong evidence exists of a nonuniform elemental composition profile at the surface for many multi-element alloy specimens, which is significantly different from the bulk composition.[1-3] Such a composition nonuniformity adversely affects the measurement of basic materials properties in alloys. Assembly of a set of disparate alloying elements into one multi-element alloy by pyrometallurgy is fundamentally a complex process due to element-specific thermophysical properties, inter-elemental interactions and the history dependence of surface morphology. Container walls as well as trace-level impurity particles mediate nucleation of crystallites in the melt that are varied in morphology.[4,5] Our investigation suggests that a depth-resolved elemental composition profile may in fact exist even for pure specimens due to accumulation of trace-level impurity elements at the surface.

The resulting nonuniformity has myriad consequences, including large variations in surface emissivity and corrosion/wear characteristics and depth-dependent thermophysical properties. In this paper we present a new study of the processes by which such depth-dependent near-surface elemental composition develops. A low melting point metallic alloy, specifically, Wood's alloy, is examined as a model system under varying thermal conditions within a vacuum chamber. The study makes use of the method of time-resolved spectroscopy of the emissions from a laser produced plasma (LPP) plume growing out of the sub-micron surface layer of the specimen. It allows simultaneous measurement of both the composition[6-8] and thermal diffusivity of the surface layer[9-11]. Repetitive LPP excitations expose the depth dependence with ten-nm depth resolution. A full set of composition and thermophysical property measurements is repeated over a range of temperature that spans from a molten state to a solid state. Successful studies include a variety of metallic alloys, solid as well as molten, ranging from stainless steel alloys[10,11], galvanized steel[3], Nichrome[1], magnetic mu-metal[12], Wood's alloy[2] and titanium thin film on a copper substrate[13]. The profiles of both the elemental composition and thermophysical properties were found to change as the thermal state of the specimen evolves over time.
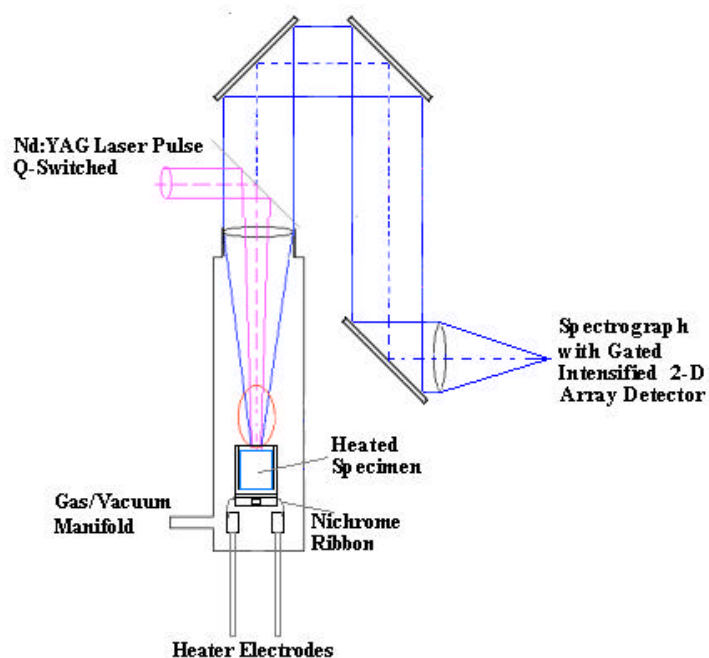
Figure 1. A schematic diagram of the specimen vacuum chamber, which is vertically positioned. At the top is the shared optics for laser beam delivery to the specimen and for collection and transfer of LPP plume emissions for quantitative spectroscopy. A high energy density dichroic mirror is used for this purpose. A spectrograph and gated intensified 2-D array detector facilitates time and space resolved measurement of the LPP plume spectrum. The specimen is contained in a crucible inside the chamber, which is supported and heated by a Nichrome ribbon heater. The chamber is filled with argon to 150 Torr during the LPP analysis runs in order to manage and suppress darkening of the optical surfaces due to alloy vapor condensation.

2. Experimental Arrangement

The experimental arrangement is shown schematically in Fig. 1. It consists of a vacuum chamber, a Q-switched Nd:YAG laser, a spectrograph equipped with a gated intensified CCD detector and a system of optics which directs the laser pulse to the specimen surface and collects emissions form a LPP plume. The laser is operated for 0.175 J pulse outputs through the entire series of experimental runs. The chamber of cylindrical shape is aligned vertically so that the specimen in a crucible can be held in place even when it is melted.

The crucible has cylindrical cup geometry, machined out of a 12.5-mm diameter rod of stainless steel 304. A Pyrex lining was also added to verify that the specimen in the melt is unaffected by the stainless steel surface. The crucible is supported and heated by a Nichrome heater ribbon. The specimen temperature is measured by means of an alumel-chromel thermocouple attached to the crucible.

The window at the top of the chamber is actually a quartz lens, which serves a dual function as a focussing lens for the laser pulse and as a collimating lens for the LPP plume emissions. A high-power dichroic mirror separates the laser pulse from the plume emissions by

reflecting the laser pulse into the chamber and transmitting the collimated plume emissions. A second lens refocuses the plume emissions onto the entrance slit of the spectrograph. The emission intensities are recorded a uv-visible spectrum by gated intensified capture of the emissions onto the CCD array detector for the duration of 320 ns starting at 400 ns from the onset of the laser pulse.

The specimen chamber was first evacuated to better than 8×10^{-6} Torr and then filled with pure argon to 150 Torr (or 2.00×10^4 Pa) before subjecting a specimen to thermal cycling. Each specimen is then heated and cooled several times over selected ranges of temperature. LPP analysis is carried out for each specimen at different temperatures during heating as well as while letting it cool.

3. Experiment Protocol

The central idea for the LPP analysis method for simultaneous determination of the elemental composition[6-8] and thermal diffusivity[9] is based on the causal relationship of the mass loss and the atomic and thermophysical properties of a given specimen. When the ablation front is driven toward the interior of the specimen in pace with the thermal diffusion front, the LPP plume becomes representative of the target specimen in elemental composition. The total mass loss by LPP ablation is determined by the local thermal diffusivity, subject to the heat of formation required for ablation and the diffusive dispersal of the atomic species entrained in the plume. The relationship has been expressed in the form of the scaling relationship: $\theta = C \, D_T{}^\alpha \, M^\beta \, H_f{}^\gamma$. Here θ denotes the thickness in cm, D_T is the thermal diffusivity in units of $cm^2 \cdot s^{-1}$, M is the molar weight, and H_f is the heat of formation in $J \cdot g^{-1}$. For a specimen in a vacuum $C = 11.07 \pm 0.45$, $\alpha = 0.91 \pm 0.01$, $\beta = -\alpha$, and $\gamma = -1$. It means that determination of both the mass loss and composition provides sufficient means to fix the local thermal diffusivity, when the advance of the ablation front is pegged to that of the thermal diffusion front by choosing laser pulse parameters.

Against this background, we focus on the evolution of the elemental composition profile as precipitated by different regimens of thermal cycling applied to Wood's alloy specimens. The Wood's alloy specimens used for this study have the manufacturer's composition of 50 W% bismuth, 25 W% lead, 12.5 W% tin and 12.5 W% cadmium.

3. Measurements and Analysis

We first follow the changes in the elemental composition in the surface layer when the specimen is heated to melting (at 71 ^{o}C) and beyond. Fig. 2 shows a sequence of the emission spectra captured from each LPP plumes. Here altogether five emission lines are used to deduce the composition and mass loss measures, one each for lead, tin, and bismuth, and two for cadmium. A sample of known composition is used to calibrate the emission line intensities for relative elemental abundance. The mass of the sample was first measured by using a digital microbalance, and it was remeasured after 300 LPP ablations were administered in argon at 150 Torr in order to assign an absolute figure for the mass lost per LPP ablation. For the calibration sample, the mass loss was found to be 5.4 μg per LPP shot, and this translates to 0.08 μm for the thickness of the surface layer removed under the given experimental condition.

wd18fmrg.i15

Heating

Cooling

Heating

1000

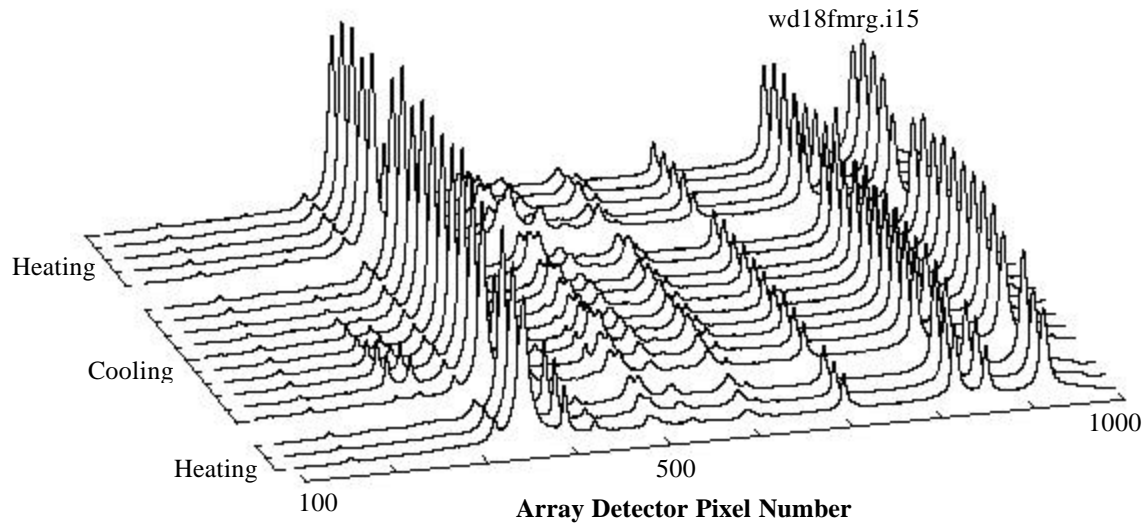500

100

Array Detector Pixel Number

Figure 2. The LPP plume emission spectra from the top surface of a Wood's alloy specimen, which has been heated to melting, followed by cooling and reheating-cooling, according to a protocol described in the text. The actual specimen temperature is shown in Fig. 3. The array detector pixel addresses are shown along the wavelength axis. The wavelength increases linearly with increasing pixel address, where pixel #348 and #920 correspond to 4057.807Å and 4799.912Å, respectively.

T, °C

200

0

Mass Loss, mg

8

0

Concentration, W%

50

0

⊗ Bismuth ▪ Lead + Tin ○ Cadmium

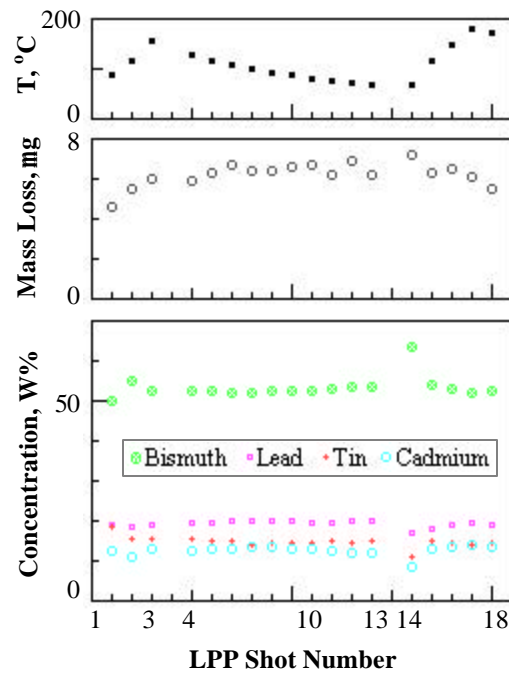1   3   4   10   13 14   18

LPP Shot Number

Figure 3. Measured elemental concentration and mass loss for the thermally cycled Wood's alloy specimen of Fig. 2. The results are derived from the set of spectra shown in Fig. 2. The following emission lines are used: 4057.807Å PbI (pixel #348) for lead; 4524.74Å SnI (pixel #702) for tin; 4722.52Å BiI (pixel #858) for bismuth; and 4678.149Å CdI (pixel #823) and 4799.912Å CdI (pixel #920) for cadmium.

4

Fig. 3 is a compilation of elemental composition in W% (Fig. 3c) and the mass loss in µg (Fig. 3b), as deduced from each of the spectra of Fig. 2. The eighteen ablations were administered during the thermal cycle of alternating heating and cooling between 65.6 ^{o}C and 177.1 ^{o}C. The succeeding LPP excitations had been separated by approximately one minute. The corresponding temperatures are also shown (Fig. 3a). We see that elemental composition exhibits modest temperature dependence while the specimen is in a molten state. When it solidifies, the composition at the surface changes sharply to a much larger extent (see the shot #14 of Fig. 3). The mass loss per LPP excitation also exhibits variability, according to the
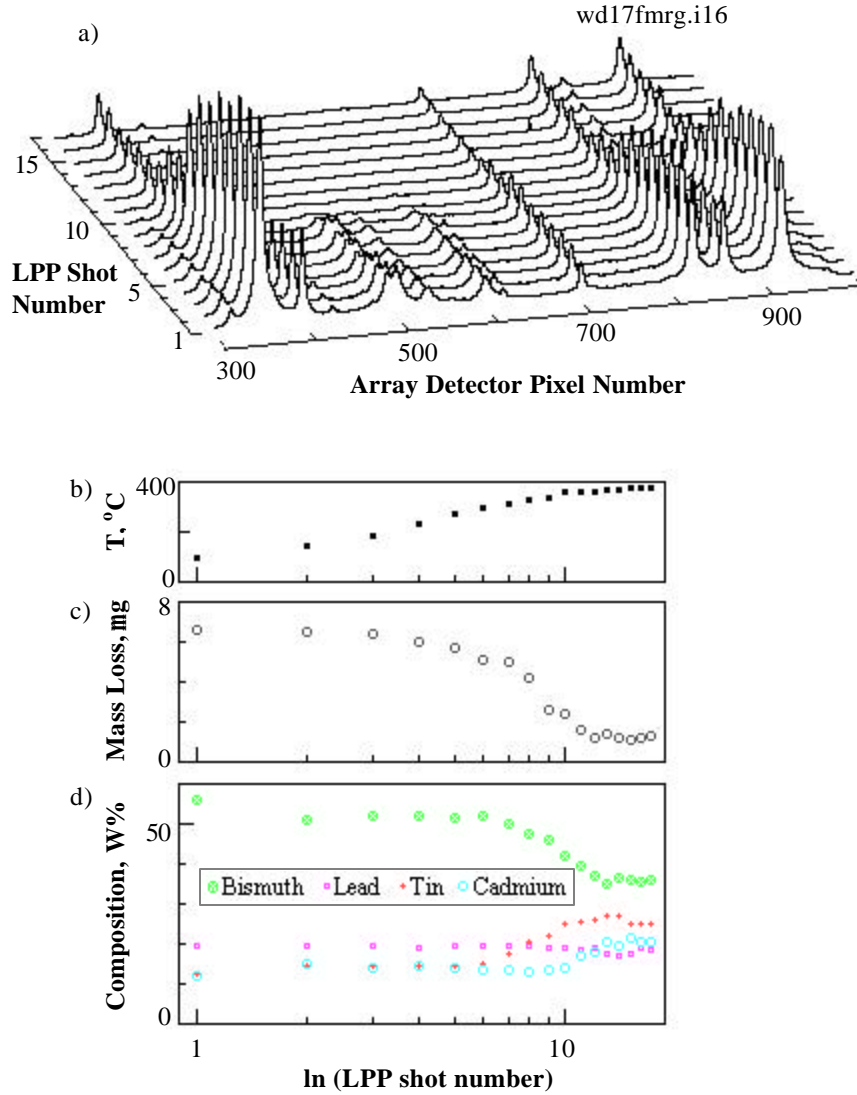

Figure 4. Seventeen consecutive LPP plume emission spectra (a) from the top surface of the Wood's alloy specimen from the runs of Fig.2, while it is reheated up to 374 ^{o}C. The actual specimen temperature (b), mass loss per LPP shot (c), and elemental composition of each LPP plume (d) are shown as functions of the LPP shot number. The shot number axis is represented logarithmically. The wavelength axis for Fig. 4a is organized in the same manner as described in the caption of Fig. 2.

composition-dependent thermophysical properties, which in turn govern the surface's response to LPP excitation.

Fig. 4 shows the surface's response to LPP excitation when the same specimen is heated again over a wider range of temperature between 93.3 $^{\circ}$C and 374 $^{\circ}$C. Altogether 17 spectra are compiled (Fig. 4a), approximately one minute apart. The resulting elemental composition (Fig. 4d) and mass loss Fig. 4c) are shown, together with the specimen temperature (Fig. 4b). This set of LPP runs reveals that the elemental composition at the surface undergoes a drastic change as the temperature rises beyond about 335 $^{\circ}$C. We emphasize that the measured composition and mass loss pertain strictly to the surface layer because as a molten specimen at elevated temperature, the area of the freshly ablated surface recovers to a new steady state by active transport of constituent elemental species into the surface layer.

Another new specimen was prepared by cycling through heating and cooling according the following schedule: heated to 152 $^{\circ}$C, cooled to 29 $^{\circ}$C, heated to 204 $^{\circ}$C, cooled to 153 $^{\circ}$C and heated again to 371 $^{\circ}$C. The specimen then resolidified when allowed to cool to 46 $^{\circ}$C before carrying out the LPP analyses. Fig. 5 shows a set of LPP plume emission spectra selected from 300 consecutive LPP analysis runs performed on the specimen. These spectra now represent the composition and mass loss analysis as a function depth from the resolidified specimen surface. It is worth noting that the heating history includes the specimen temperature exceeding the threshold temperature at about 335 $^{\circ}$C. The near surface composition has been irreversibly changed from the initial composition of the fresh specimen. Attempts of further heating have failed to restore the near-surface composition to that of the fresh specimen.
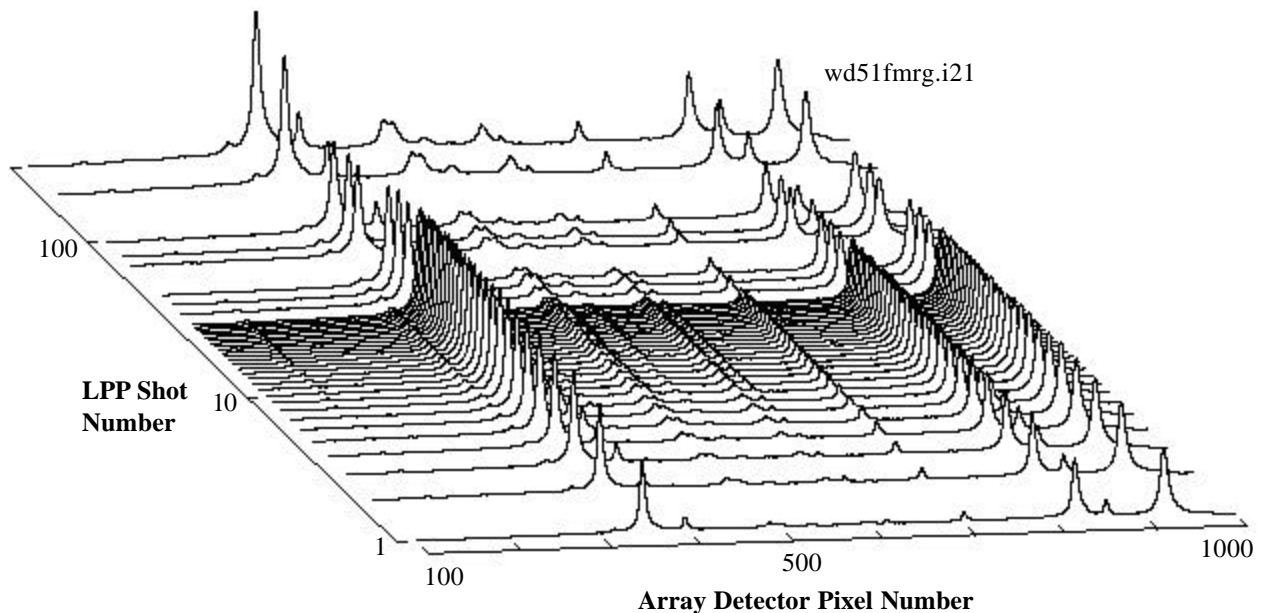

Figure 5. Selected LPP emission spectra from a 300-shot sequence of LPP analysis carried out for a Wood's alloy specimen in a solid form at near room temperature. The specimen had been processed through three rounds of heating and cooling. The detail history of thermal cycling is given in the text. The highest specimen temperature was 371 $^{\circ}$C. The wavelength axis is organized in the same manner as described in the caption of Fig. 2.

Fig. 6 shows at each LPP excitation the thickness of the specimen layer ablated by the laser pulse (Fig. 6a), the mass removed (Fig. 6b) and the elemental composition in W% (Fig. 6c) of the layer removed. The elemental compositions of the outer surface layers are dramatically different from that of the bulk. The surface is strongly dominated by cadmium at
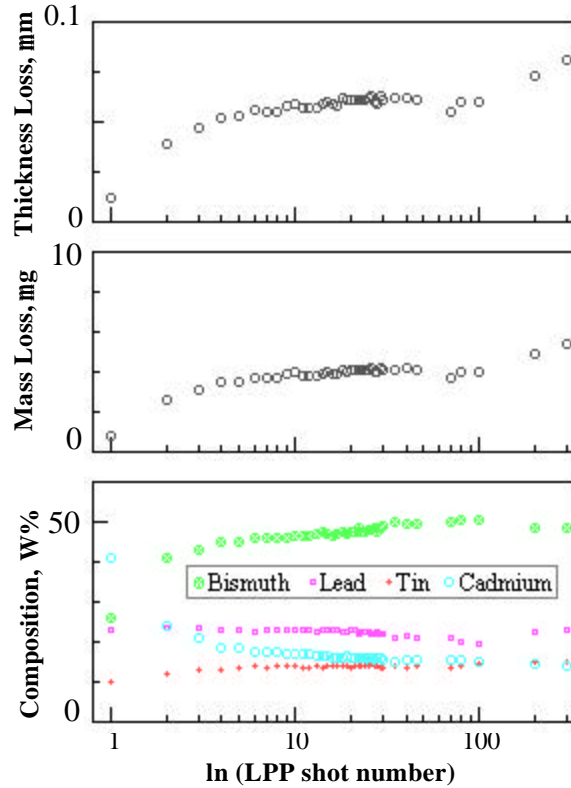

Figure 6. A compilation of the measured elemental concentration (c), mass loss (b) and the thickness of the specimen layer removed for each LPP ablation for the thermally cycled Wood's alloy specimen of Fig. 5. The results are derived from the set of spectra shown in Fig. 5, according to the procedure described in the caption of Fig. 3 and in the text.

the expense of bismuth. This reversal of the respective concentrations of the two elements is plausible from the standpoint of the fact that the cadmium is the lightest of the four constituent elements in the specimen where as bismuth is the heaviest. Both gravity and atomic diffusion would favor the emergence of cadmium to the top surface. In another earlier study of Wood's alloy, we examined development of a depth dependence in near-surface elemental composition by melting a Wood's alloy specimen and holding it for a period of time before letting it cool to resolidify in the presence of gravity[2]. The temperature of the melt was kept within 20 ^{o}C from the melting point. This modest heating resulted in a slight enrichment of lighter elements at the top surface. The present result suggests that the contribution from atomic diffusion becomes an increasingly significant player as the temperature is further increased. The concentration of lead is less affected than that for bismuth, suggesting that the strong wetting property of lead, may be another one of the determining factors.

4. Concluding Remarks

Using Wood's alloy specimens as a model alloy system, we have demonstrated the existence of a significant causal relationship between the thermal history of an alloy specimen and its near-surface composition profile. The central issue here has to do with the fact that many thermophysical properties one measures for a given material specimen are strongly influenced by near-surface elemental composition while the near surface composition can be driven away from the bulk composition by myriad processes. One prominent process is heating, and the exact thermal history of a given specimen in the course of alloy refinement, melting and resolidification, specimen preparation, storage and its interaction with measurement instrumentation contributes to the eventual outcome of near-surface composition and morphology. We have observed that the thermal history may have an irreversible effect on the near-surface composition of the specimen. The case in point is the existence for the Wood's alloy specimens of a threshold temperature of about 335 $^{\circ}$C, beyond which the near-surface composition is driven irreversibly away from the bulk composition.

Central to our investigation is the ability to track the surface composition in-situ. We have relied on the unique capability accorded by the LPP analysis to simultaneously measure both the composition and thermal diffusivity. In the case of solid specimens, depth-resolved measurement is possible because excitation of an LPP plume entails removal of a thin layer of surface matter from the surface, exposing a new surface underneath. On the other hand, when the specimen is in a molten state, the surface is refreshed soon after an LPP ablation due to atomic transport processes commensurate with the state of molten matter, given a sufficient duration of time for the processes to evolve.

The physics responsible for the evolution of the near-surface elemental composition is many-fold and most likely very complex. One of the mechanisms may involve ordering of atoms into several planar layers near the free surface when a pure or binary alloy is in a molten state[14,15], and they may frozen into a solid. It is conceivable that these layers compete between elements, resulting in near surface composition that is distinctly separate from that of the bulk. The relevant processes here are affected by disparate elemental attributes such as atomic diffusion properties unique to constituent atomic masses, elemental density, wetting properties stemming from inter-particle interaction potentials, to name just a few. In our present study of the chosen model system, we have identified a control parameter, according to which different processes come into play. The existence of the threshold temperature at about 335 $^{\circ}$C for the Wood's alloy system is both telling and intriguing. This threshold temperature is just above the highest melting point among four constituent elements - namely, the melting point (326.2 $^{\circ}$C) of lead.

References

1. Y.W. Kim, *Int'l J. Thermophysics* **23**:1103 (2002).
2. Y.W. Kim, *Int'l J. Thermophysics* **23**:1171 (2002).
3. Y.W. Kim, *Int'l J. Thermophysics* **20**:1313 (1999).
4. B. T. Bassler, W. H. Hofmeister, R. J. Bayuzick, R. Gorenflo, T. Bergman, and L. Stockum, *Rev. Sci. Instr.* **63**:3466 (1992).

5. B. T. Bassler, R. S. Brunner, W. H. Hofmeister, and R. J. Bayuzick, *Rev. Sci. Instr.* **68**:1846 (1997)
6. Y.W. Kim, in *Laser-Induced Plasmas and Applications*, L.J. Radziemski and D.A. Cremers, eds. (Marcell Dekker, New York 1989). Chapter 8.
7. Y.W. Kim, *High Temp. Sci.* **26**:57 (1990).
8. Y.W. Kim, U.S. Patent Number 4,986,658 (22 January 1991).
9. Y.W. Kim, *Int. J. Thermophys.* **14**:397 (1993).
10. Y.W. Kim and C.-S. Park, *Int. J. Thermophys.* **17**:713 (1996).
11. Y.W. Kim and C.S. Park, *Int. J. Thermophys.* **17**:1125 (1996).
12. Y.W. Kim, "Composition-Profile Basis of Depth-Dependent Thermophysical Properties," (in press).
13. Y.W. Kim, *Int. J. Thermophys.* **23**:1091 (2002).
14. H. Tostmann, E. DiMasi, O.G. Shpyrko, P.S. Pershan, B.M. Ocko, and M. Deutsch, *Ber. Bunsenges. Phys. Chem.* **102**:1136 (1998).
15. E. DiMasi, H. Tostmann, O.G. Shpyrk, M. Deutsch, P.S. Pershan and B.M. Ocko, *J. Phys.: Condens. Matter* **12**:A209 (2000).